Association Aéronautique et Astronautique de France

57th 3AF International Conference on Applied Aerodynamics
29 — 31 March 2023, Bordeaux – France

AERO2023-24-RUBERTE

BELLY-FAIRING DESIGN SPACE EXPLORATION FOR A FORWARD SWEPT NATURAL LAMINAR FLOW AIRCRAFT

Javier Ruberte Bailo[1] Arne Seitz[2] and Thomas Streit[3]

[1]*German Aerospace Center (DLR), Braunschweig, 38108 Germany, Javier.RuberteBailo@dlr.de*

[2]*German Aerospace Center (DLR), Braunschweig, 38108 Germany, Arne.Seitz@dlr.de*

[3]*German Aerospace Center (DLR), Braunschweig, 38108 Germany, Th.Streit@dlr.de*

ABSTRACT

A Natural Laminar Flow, forward swept wing with a lift coefficient of 0.52, a wingspan of 34 meters and an aspect ratio of 9.47 for a Reynolds number of 23.83 Million and a Mach number of 0.78 has been developed during the TuLam/EcoWing projects. In order to tackle wing-fuselage interaction, a new belly-fairing has been designed. The belly-fairing is based on parameterized B-Splines in Catia. On the present study a characterization of the most important parameters and their influence in performance metrics has been assessed and refined by the surrogate model approach with SMARTy. The meshes have been generated with SOLAR and the RANS solver TAU has been used for the simulations. The results show the high degree of influence that the belly-fairing has in the overall performance. Some geometries achieve a glide ratio close to 23.5 for cruise conditions with free transition and 20.5 with 5% tripped transition.

1. NOMENCLATURE

ALT	Attachment line transition
BSW	Backward swept wing
c	chord
CF, CFI	Cross flow, cross flow instabilities
C_L,C_D	Lift and drag coefficient
C_P	Pressure coefficient
C_P*	Critical pressure coefficient
CS	Cross section
C_x	Force coefficient in the *x* direction
C_y	Force coefficient in the *y* direction
ΔV	Transversal speed variation due to displacement effects
d.c.	Drag counts 0,001 C_D
DOF	Degrees of freedom
$E = C_L/C_D$	Glide ratio
η_{BF}	Non-dimensional position of the given CS
FSW	Forward swept wing
Ma	Mach number
MAC	Mean aerodynamic chord
NLF	Natural laminar flow
ϕ, ϕ_{eff}	Geometrical and effective sweep angle
R1	Ratio 1
R2	Ratio 2
RA	Reference angle
Re	Reynolds number
TS, TSI	Tollmien-Schlichting, Tollmien-Schlichting instabilities
V_∞, V_N, V_T	Free-stream, normal and transversal velocity
x, y, z	Aircraft fixed coordinate system
YR	Y ratio
ZR	Z ratio

2. INTRODUCTION

Reduction of greenhouse emissions is and has been for a long time a strong motivation for the aerospace industry to pursue efficiency improvements, furthermore, due to the current energy crisis that the world currently faces and the high cost associated to new propulsion technologies, such as hydrogen or synthetic fuels, the energy consumption reduction of aircraft is imperative .

Laminar flow is one of the most promising technologies in current development due to the potential for high reduction in drag that the technology offers, but at the same time, as history has proven, it is not a straight for-

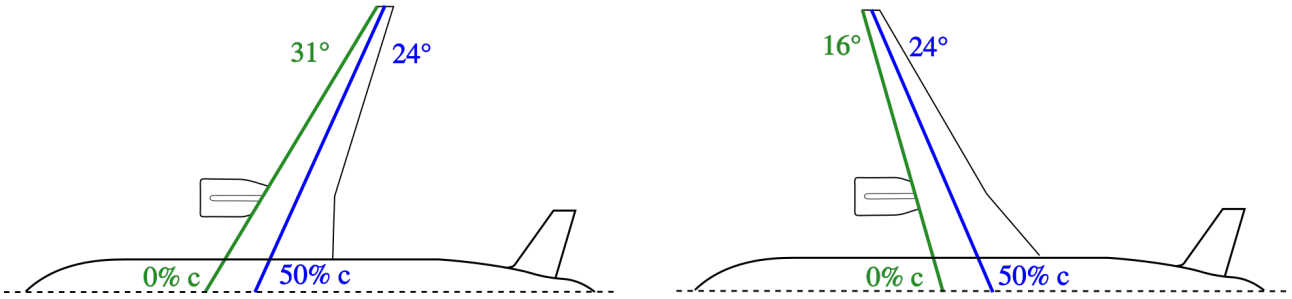

Figure 1: Influence of the configuration in the leading edge sweep for a given re-compression shock sweep in a tapered swept wing. While both configurations offer a 24° sweep at the re-compression shock region, the forward swept wing offers a much lower leading edge sweep which leads to lower cross-flow instabilities and therefore better laminar conditions. Sketch based on Seitz [12]

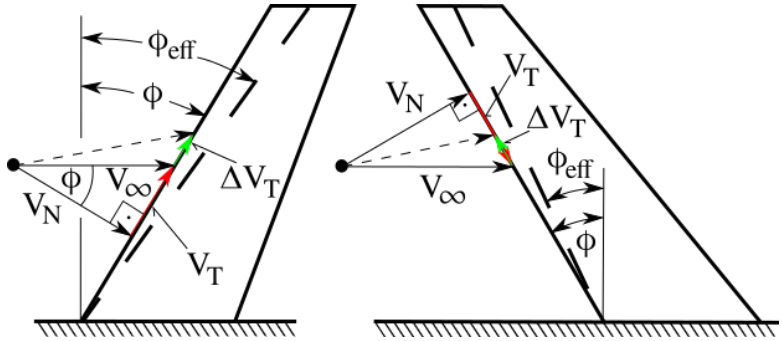

Figure 2: Influence of the displacement in a tapered swept wing. The displacement reduction along the wingspan due to the taper causes a variation of the transverse velocity ΔV_T, which adds to the Transverse velocity in BSWs and subtracts for FSWs, causing an additional effective sweep in a BSW and a reduced effective sweep in a FSW. Sketch based on Redecker and Wichmann. [8]

ward technology to be implemented. Laminar flow is present in subsonic aircraft such as sailplanes or some private aircraft such as the HondaJet [4] or the Piaggio P.180 [13], but it has not yet been implemented in larger transport aircraft.

The required laminar technology for regional, low Mach number turboprop aircraft such as the Do328 or the ATR 42 is available since many years [14]. Transonic middle range aircraft such as the Airbus A320 family or the Boeing 737 do have more complex flows, but as will be discussed are also feasible. As the european aviation environmental report 2022 shows [1], 65% of the flights and 46.3% of the CO2 emissions are generated by middle range, single aisle jets, which provides an untapped potential to reduce CO2 emissions.

The other main source of CO2 emissions are long range, twin aisle jets, which according to the european aviation environmental report 2022 [1], despite only being 6.6% of the total flights, produce 48.1% of the CO2 emissions. The European HLFC-Win project aims to demonstrate that the laminar technology for long range aircraft have reached a technology readiness level 4 [16].

The main aerodynamic obstacle towards laminar flow in middle range aircraft are high Reynolds numbers and high flying Mach number. The high Reynolds numbers makes the laminar to turbulent transition much more difficult to avoid, the high flying Mach number requires a sweep angle, which has big impact in two of the main laminar to turbulent transition mechanisms, attachment line transition (ALT) and cross-flow instabilities (CF) [7].

There are different methods to achieve laminar flow, the most straight forward method is called natural laminar flow (NLF), it is a passive method in which laminar flow is obtained by aerodynamic wing shape design. Another, more complex method is called laminar flow control (LFC) and is based in active methods to archive laminar flow, such as suction. LFC has less constrains than NLF but requires more energy and additional equipment. Additionally, there is a middle ground technology, called hybrid laminar flow control (HLFC), which uses NLF where possible and LFC were needed.

Transonic middle range aircraft need either wing sweep or thin airfoils in order to cruise with low wave drag, usually a mix of both is used since overuse of either can lead to increased structure weight. Middle range design cruise Mach number usually is 0.78, whereas long range aircraft have a cruise Mach number ranging from 0.82-0.85. Although there is some examples of forward

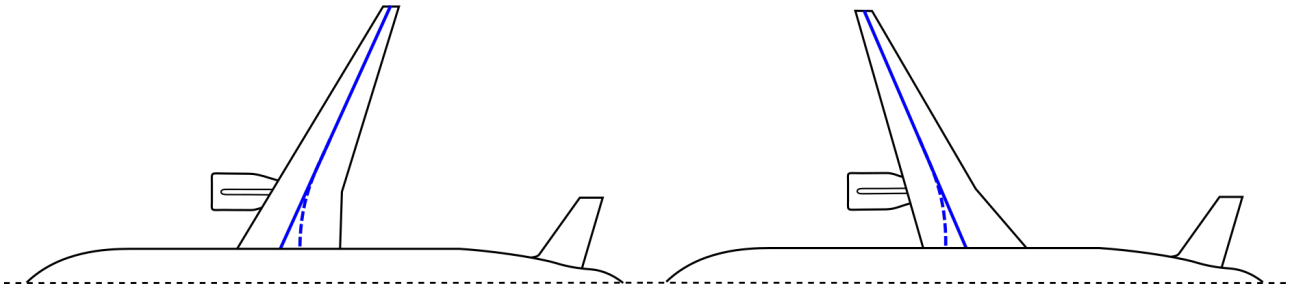

Figure 3: Representation of the middle plane effect, also known as 3D effects on the re-compression shock for a BSW and a FSW configuration at the wing root. The solid line represents the ideal isobar distribution, the dashed line represents the shock position found if no 3D integration takes place, which is characterized by a large region with a normal re-compression shock and a high wave drag.

swept wings (FSWs) such as the HFB 320 [3], most transonic aircraft have backward swept wings (BSWs), the reason is that, for a turbulent configuration with a proper designed pressure distribution, BSWs are enough to obtain low wave drag configurations, furthermore due to the isotropic metal wings BSWs offer an aeroelastic advantage against FSWs. Since modern composite wings can be tailored to counteract aeroelastic disadvantages [5] and FSWs provide fundamental advantages towards NLF, FSWs are being considered for next generation aircraft.

FSWs offer better conditions than backward swept wings for NLF in a transonic configuration with tapered swept wings. For a given, moderate re-compression shock sweep angle, necessary to achieve low wave drag with NLF airfoils, with an optimal isobar pressure distribution, FSWs have lower leading edge sweep, which limits the growth cross-flow instabilities and prevents attachment line transition. Fig. 1 provides an overview of the influence of the configuration in the leading edge sweep and the re-compression shock sweep. Furthermore, FSWs offer an advantage against BSWs, since, as Redeker and Wichmann [8] found out, FSWs reduce effective sweep at the leading edge, which further reduces the risk of CF and ALT transition. Fig. 2 shows the effects of displacement on the effective sweep angle for BSWs and FSWs.

NLF profiles are characterized by a constant acceleration, followed by a re-compression shock which is usually found between 50 and 65 % of the chord length. the constant acceleration is necessary in order to keep Tollmien-Schlichting (TS) instabilities under control, the re-compression shock is common method used to bring the highly accelerated supersonic flow back to subsonic flow, which has to be carefully balanced with the laminar flow drag reduction and the local sweep angle to provide an overall benefit. In order to achieve low wave drag despite the re-compression shock, a moderate sweep is necessary in the re-compression region. Since laminar profiles need a moderate sweep angle in the re-compression shock and a low sweep angle in the leading edge, for tapered FSWs arise as a straight forward method to design NLF wings.

Due to the re-compression shock found in laminar profiles, a mindful 3D integration is necessary in the 3D regions found at the wing root and wing tip, as the de-sweep known as middle plane effect can increase the wave drag substantially, as Streit and Hoffrogge found out [15], the middle plane effect causes for BSWs a more gradual gradient in the first half of the profile and a sharper gradient in the second half of the profile. FSWs are affected the other way around. As it can be observed in Fig. 3, the middle plane effect has also an influence in the re-compression shock position, due to the middle plane effect, the re-compression shock tends to run normal to the fuselage and has also a large section perpendicular to the oncoming flow, which is coupled together with high wave drag due to the low local sweep. Furthermore, the normal re-compression shock can also lead to phenomena such as double shocks or flow separation.

In order to tackle the middle plane effect, 3D inverse design methods are a tremendous help, as the designer provides the desired pressure distribution and the 3D inverse method finds the necessary geometry accounting for the 3D effects. Nevertheless, as Streit and Hoffrogge found out [15], the middle plane effect has such intensity, that big geometry modifications may be needed in order to achieve the same pressure distribution as outside of the 3D region. However, due to the geometry restrictions, middle plane effects can only be partially mitigated.

In order to provide a proper 3D integration at the wing root and counteract the middle plane effect, Belly fairings can be designed to support the wing gradients. At the current time, there is no simultaneous inverse design method for the wing and the belly fairing available, therefore usually an iterative process is necessary in which a 3D inverse designed wing is coupled with a generic, parametric belly fairing, then an appropriate geometry of the belly fairing is searched which at wing fuselage root leads to similar pressure distributions as the ones found

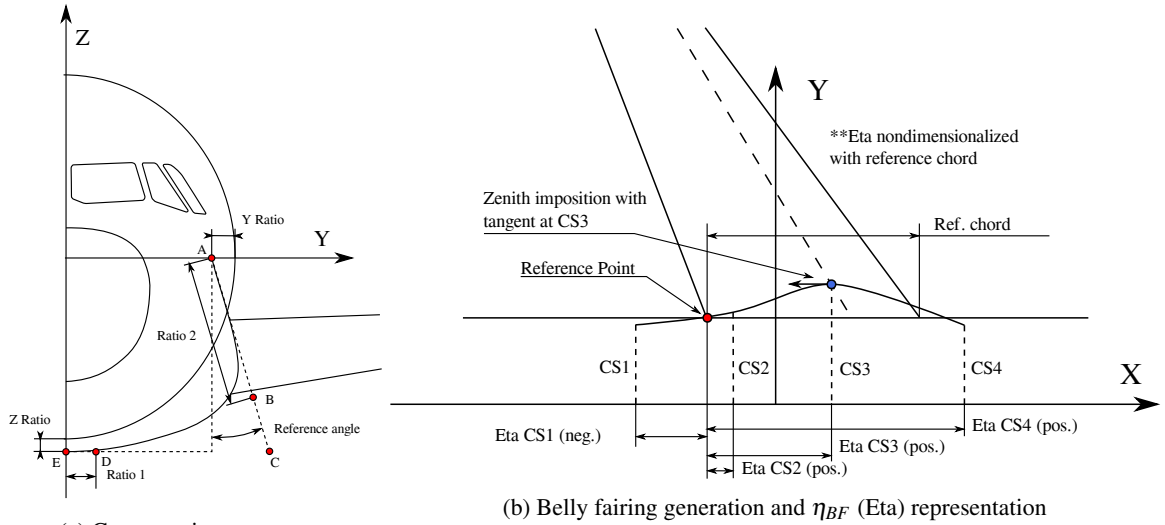

(a) Cross-section parameters

(b) Belly fairing generation and η_{BF} (Eta) representation

Figure 4: Representation of the methodology used to generate the belly fairing, on the left, the cross section generation with the parameters used, on the right, the alignment of the cross sections to generate the belly fairing.

for spanwise sections lying more outboard.

During the DLR Project TuLam a Forward Swept Wing NLF configuration was designed by Seitz et al. [12]. In order to provide an appropriate pressure distribution in the influence region of the fuselage a new belly faring was necessary. Therefore a parameterized belly fairing design has been explored in this work. The parametric geometry allows to assess the level of influence that each parameter has over the performance, and to single out the parameters according to the desired influence. Additionally a data set of belly fairings has been built which allows to correlate the performance metrics with the flow phenomena. The impact of the belly fairing has been compared using performance metrics such as laminar overall drag, wave drag, shock de-sweeping and turbulent overall drag in order to determine which belly fairing is best performing. Turbulent performance at cruise conditions has been also considered to choose the best performing geometry.

3. METHODOLOGY

3.1 Flowfield

The TuLam/EcoWing configuration is a FSW-NLF configuration with similar top level aircraft requirements as the Airbus A320. It is a clean configuration for cruise flight without tail-plane or engines, wing area is 122 m^2, wing span is 34 m and the aspect ration is 9.47. The leading edge sweep is -17°, the trailing edge sweep is -27.8° and the sweep at the 65% chord length is -24°. The cruise lift coefficient is 0.52, the cruise altitude is FL370 and the cruise Mach number is 0.78. The Reynolds number is 23.83 Million at the mean aerodynamic chord.

3.2 Belly fairing generation

In order to parameterize the belly faring a cross-section methodology developed by Ronzheimer [9] has been used. The software used for the belly fairing generation is catia v5. Each of the cross sections are contained in a plane normal to x-axis as Fig. 4b shows and can be moved along the x-axis with the η_{BF} (Eta) parameter. The η_{BF} parameter has been non-dimensionalized with the reference chord length and uses the intersection of the wing and the cylindrical fuselage as reference point. Four parameterized B-spline cross sections (CS) have been used to generate a multi section surface. As Fig. 4a shows, each of the cross-sections is a 4th degree B-spline with 5 points. The points have been constrained in a way that only 6 parameters are necessary to vary the B-spline geometry. In total, the 4-cross-section belly fairing has 24 degrees of freedom (DOF). In order to reduce the number of DOF, the work has been limited to the parameters that influence the suction side of the two inner cross-sections. That is to say, η_{BF}, Y Ratio (YR) and Reference Angle (RA) of the cross-sections 2 and 3. Furthermore, since the third cross-section is closest to the re-compression shock, it was decided to lock the Y Ratio of the third section at the lowest (thickest belly fairing in this region) value possible of 0.001. By doing this the total number of DOFs was reduced to 5.

3.3 Mesh generation

Due to the high degree of influence that the re-compression shock has in the overall performance and the high degree of influence that the discretization has on the re-compression shock, it was decided to perform high fi-

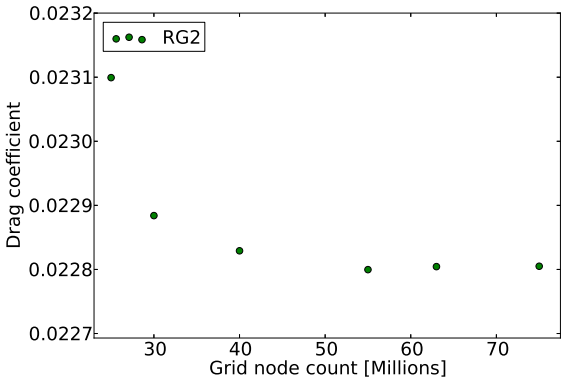

Figure 5: mesh independence study

delity simulations. In order to simplify the meshing step no mesh adaptation was used. The meshes were done with SOLAR [6] and a grid independence study was performed, the results of the study can be observed in Fig. 5. The number of nodes chosen were 55 million for a half-model.

3.4 Solver and sampling strategy

The DLR RANS solver TAU [11] was used for the simulations, the simulations were performed with the Spalart-Allmaras turbulence model and the transition module of TAU based on the e^n method, Coco and Lilo [10].

Due to the novelty of the configuration, no previous data was available regarding suitable parameters for the belly faring generation. In order to generate an initial parametric belly fairing, a preliminary study was performed, in which the parameter limits were explored. An available belly fairing from previous work in DLR [9] was adapted.

In order to fit the simulation domain a fully factorial simulation was performed. The simulation domain was then expanded according to the results obtained in an iterative manner where good performance was observed.

Once the simulation domain was obtained, the surrogate approach was implemented in order to find good performing geometries in an efficient manner due to the high cost of the high fidelity simulations. The Surrogate model was performed with the DLR software SMARTy [2].

The fixed parameters chosen are displayed on Tab. 1. The limits of the explored parameters are shown in Tab. 2.

3.5 Post processing

In order to choose the best performing geometries, different strategies have been used. The angle of attack, lift and drag coefficients are of foremost importance and have been heavily weighed. Also wave drag has been consid-

belly fairing fix parameters						
CS	η_{BF}	YR	RA [deg]	R2	ZR	R1
1	-0.5	0.2	4	0.25	0.082	0.25
2	n/a	n/a	n/a	0.8	-0.056	0.7
3	n/a	0.001	n/a	0.8	-0.01	0.8
4	1.4	0.1	8	0.3	0.2	0.357

Table 1: Fixed parameters in the belly fairing

Limits of the variables		
Variable	min.	max.
η_{BF2} [/]	0	0.3
Reference angle 2 [deg]	2	10
Y Ratio 2 [/]	0.012	0.07
η_{BF3} [/]	0.55	0.95
Reference angle 3 [deg]	0	10

Table 2: Limits of the variables used for the belly fairing generation

ered, due to the role that it plays in this work and the high correlation between wave drag and drag rise Mach number. In order to obtain the wave drag coefficient, a post processor by Streit et al. [17] has been implemented. Although the post processor is very useful, it can only recognize one re-compression shock, which leads to underestimate the wave drag in geometries with a double re-compression shock. Geometries in which a large second shock is found, are not desired in the first place but it is important to note this limitation. The wave drag for geometries with a double re-compression shock have been noted in the results with the * superscript to denote that the value is underestimating wave drag. In order to analyze the flow field, Tecplot macros have been developed to generate automatically figures of pressure distributions and surface contours of pressure coefficient and laminar extent. Together with the pressure distributions the output of the stability analysis, the CF and TS N-factors envelope, the transition position and the C_P* has been drawn. All this info has been plotted at the span positions where the generated airfoils are located in order to compare the influence of the belly fairing. In order to show the re-compression shock de-sweep the desired 65% position re-compression shock position has been plotted in the contour figures.

4. RESULTS

The methodology chosen has generated a few geometries with outstanding performance, additionally the study has also shown the level of influence that the belly fairing has in the overall performance. Tab. 3 shows the performance of some of the best performing geometries under laminar flow, additionally, Geo762, one of the bad per-

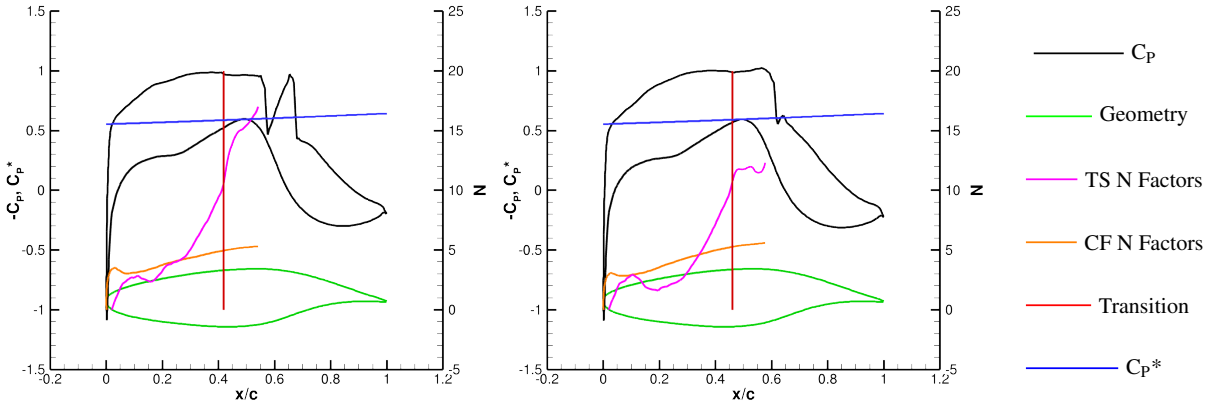

(a) Geo432 (b) Geo594

Figure 6: Comparison the C_P distribution between Geo432 and Geo594 at $\eta = 0.16332$ (position shown as a green line in in Fig. 7, Fig. 8 and Fig. 9). Geo594 is a very good performing geometry with a single shock, Geo432 is a good performing geometry but has a double re-compression shock with higher wave drag.

forming geometries has been also included, to show the level of penalty that can be expected from a bad geometry. It is worth to mention that although Geo762 shows bad performance and has flow separation at the wing root, it still achieves the design C_L of 0.52. The results show also, that a bad belly fairing can have a large re-compression shock induced flow separation which lead to an even higher lift loss and therefore the design C_L can no longer be achieved.

The shown geometries have also been simulated under turbulent conditions, which is also of major importance as during the operation of the aircraft contamination could lead to early transition. Although the performance loss is evident, accounting to an increment of drag between 32 and 35 d.c., all the good geometries show performance close to what could be expected from a classic turbulent BSW for the chosen aspect ratio of 9.47. The turbulent performance of the different geometries can be observed in Tab. 4. With turbulent flow Geo762 no longer achieves the design C_L.

Laminar performance metrics					
Name	α [deg]	C_L	C_D	C_{DW}	E
Geo267	0.763	0.5201	0.02208	0.0010	23.557
Geo294	0.772	0.5201	0.02215	0.0010	23.481
Geo301	0.799	0.5201	0.02237	0.0011*	23.254
Geo356	0.814	0.5200	0.02229	0.0008*	23.330
Geo357	0.785	0.5201	0.02225	0.0010*	23.375
Geo358	0.781	0.5201	0.02223	0.0009*	23.399
Geo432	0.818	0.5201	0.2240	0.0010*	23.219
Geo594	0.758	0.5201	0.02204	0.0008	23.598
Geo598	0.756	0.5201	0.02212	0.0012	23.509
Geo762	1.915	0.5195	0.03588	0.0025*	14.478
Geo777	0.760	0.5201	0.02211	0.0009	23.524

Table 3: Laminar performance metrics of the geometries with a laminar gliding ratio over 23. Note: all C_{DW} values with the * superscript are geometries with a double re-compression shock, due to the limitations of the post processor used, the values of C_{DW} in this geometries is underestimated

4.1 Belly fairing influence

In order to understand what kind of influence do the belly fairing have in the performance of the aircraft, a very good performing geometry, Geo594 has been chosen and it is compared with another, also good performing geometry, Geo432.

Fig. 6 shows the pressure distribution of both geometries for an inner wing section at an wingspan of $\eta = 0.16332$. The result show that the CF instability does not lead to transition, this being one of the advantages of FSWs. Geo594 has a single shock while Geo432 has a double re-compression shock. Furthermore, as it can be observed in Fig. 7, the middle plane effect is more present in Geo432, that is to say, the re-compression shock is further away from the desired 65% position, which is represented with a dashed red line, for a larger region than Geo594. Fig. 8 shows the laminar extent of both geometries, and only small differences can be found, which leads to believe that the 4 d.c. difference between Geo594 and Geo432 are mostly due to the double re-compression shock. Apart from Geo594 and Geo432 also Geo762 is shown, which as previously mentioned, is being displayed to show to what kind of influence can a bad belly fairing lead. As Fig. 9 shows, Geo762 has for a large

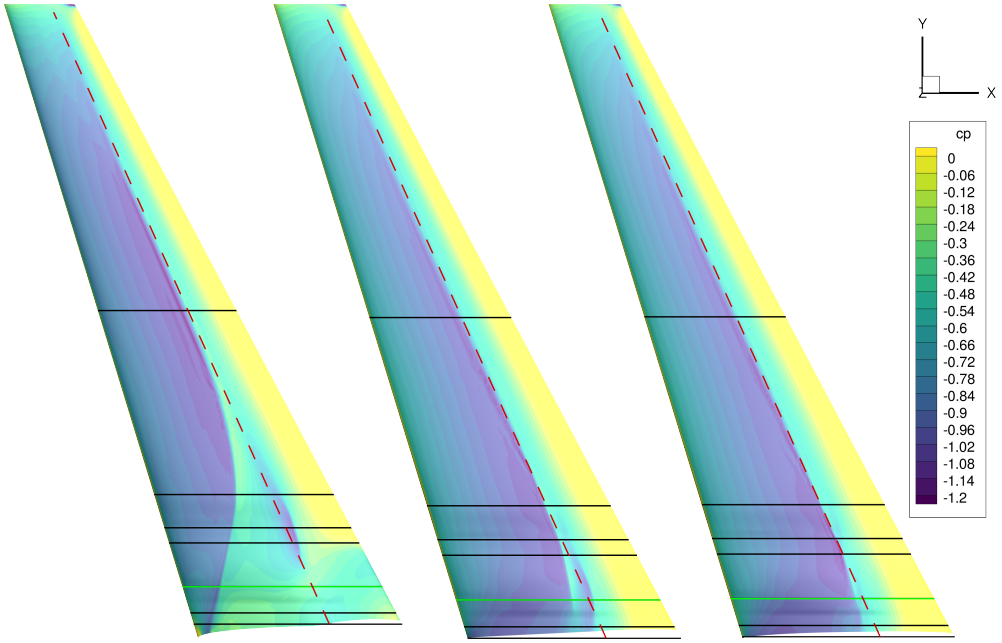

(a) Geo762 (b) Geo432 (c) Geo594

Figure 7: C_P Contours of Geo762, Geo432 and Geo594. Geo594 and Geo432 are both good performing geometries with small differences in the wing root. On the other hand, Geo762 is a bad performing geometry with a strong re-compression shock with a large region normal to the free-stream and flow separation in the inner region of the wing. For all geometries the wing is the same, only the belly fairing is different. All geometries achieve the design C_L of 0.52. The C_D is 0.03588 for Geo762, 0.02240 for Geo432 and 0.02204 for Geo594.

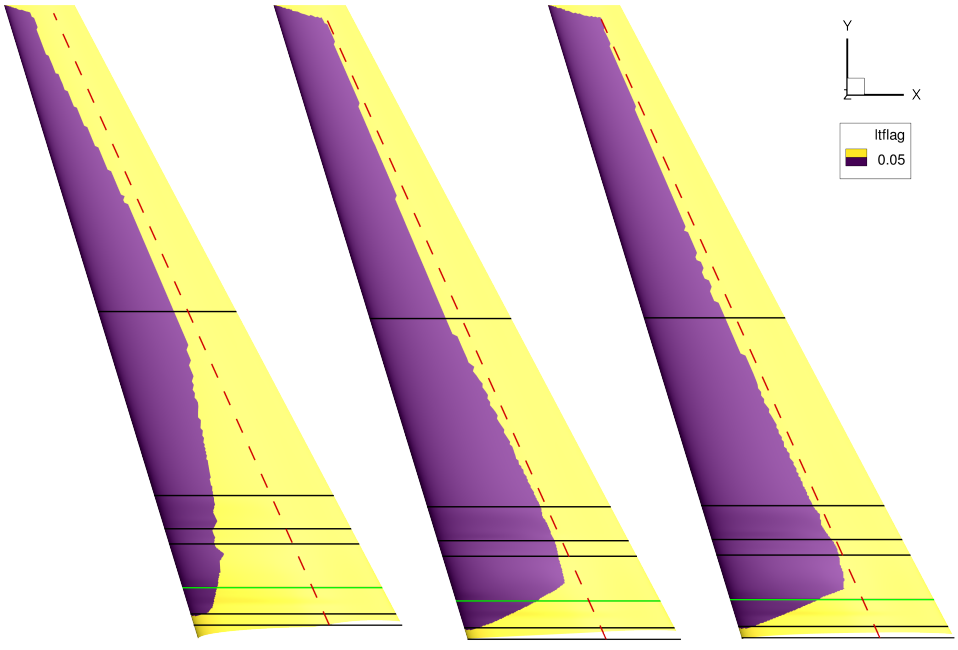

(a) Geo762 (b) Geo432 (c) Geo594

Figure 8: Laminar region in Geo762, Geo432 and Geo594. Geo432 and Geo594 show a very similar laminar region, Geo762 on the other hand shows a strong reduction of the laminar region due to the advance of the re-compression shock. The 4 drag counts difference between Geo594 and Geo432 are mostly due to the differences in wave drag, since only small differences are found in the laminar extent.

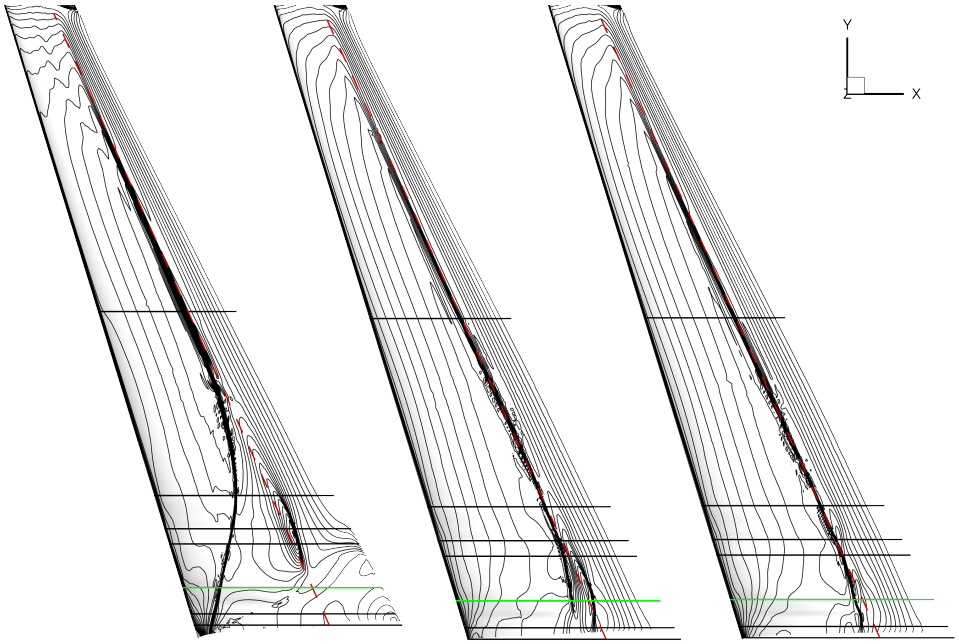

(a) Geo762 (b) Geo432 (c) Geo594

Figure 9: C_P Level lines of Geo762, Geo432 and Geo594. Geo594 shows an single re-compression shock and Geo432 shows a double re-compression shock in the wing root. On the other hand, Geo762 shows a large region with a re-compression perpendicular to the oncoming flow.

Turbulent performance metrics				
Name	α $[deg]$	C_L	C_D	E
Geo267	1.258	0.5199	0.02528	20.570
Geo294	1.261	0.5199	0.02530	20.547
Geo301	1.277	0.5199	0.02545	20.428
Geo356	1.300	0.5200	0.02552	20.378
Geo357	1.270	0.5199	0.02538	20.481
Geo358	1.272	0.5199	0.02538	20.484
Geo432	1.301	0.5199	0.02560	20.309
Geo594	1.274	0.5198	0.02553	20.355
Geo598	1.251	0.5199	0.02531	20.536
Geo762	1.414	0.4800	0.02977	16.122
Geo777	1.256	0.5199	0.02523	20.608

Table 4: Turbulent performance metrics of geometries with a laminar gliding ratio over 23

portion of the wing, a re-compression shock with little to none sweep, furthermore as can be seen in Fig. 8 due to the early position of the shock the laminar region has been greatly reduced, and as flow analysis shows, the is separated flow after the shock. All three effects combined lead to the bad performance of Geo762.

5. CONCLUSION

The main goal of the work of finding a suitable belly fairing for the new DLR FSW-NLF configuration and evaluating performance metrics for high fidelity methods has been completed, furthermore, a data set of good performing geometries has been generated which enables further research in more complex belly fairings and more complex design strategies with higher DOFs. Additionally, the results of the work show, the level of influence of a belly fairing, which can diminish all the advantages of a good performing laminar wing to the point that it is no longer able to achieve cruise flight conditions if it is not properly designed.

The best performing belly fairings show a turbulent performance similar to what could be expected from a turbulent BSW, that is to say a NLF aircraft can still operate when for operational reasons the surface is contaminated to the point of early transition over the whole wing.

Further work in belly fairing design may still lead to some performance gains as it has been shown that the

middle plane effect is still present in Geo594.

The results for the current configuration show astonishing performance, even more if considering that the aspect ratio of the configuration is 9.47, similar to current flying aircraft. If new generation geometries are considered, with higher aspect ratios and reduced mean aerodynamic chord (MAC), lower Reynolds number will be operated in cruise flight, which will enable expanding NLF different scenarios, such as:

- Higher cruise speeds with NLF. Current aerospace development shows a strong tendency towards single aisle long range flights, a product of this development is the Airbus A321XLR, which could profit from higher, optimal cruise speeds for this kind of mission as the ones found in the Boeing 757, with the additional advantage of NLF and reduced fuel consumption.
- Improved laminar off-design performance for lower flight level. While on climb flight, the decreasing density leads to a decreasing Reynolds number, therefore, although laminar flow can be found in the wing tips already early climbing phase, the full potential of laminar flow is found in cruise conditions or cruise off-design. Lower MAC would expand the laminar advantages during climb and descent phases, which translates in better laminar performance in short to medium range flights.
- Better cruise laminar performance, reduced Reynolds number lead to lower sensitivity to CFI, TSI and ALT, depending on the the mission of the aircraft, the laminar envelope could be expanded as just explained above or better performing airfoils could be designed, the lower Reynolds number allows to counteract the TSI with lower suction gradient, which leads to smaller re-compression shocks therefore lower wave drag.

REFERENCES

[1] European aviation environmental report 2022. 2022.

[2] P. Bekemeyer. Internal report. 2019.

[3] Hamburger Flugzeugbau. Sweptforward wings for the HFB 320 Hansa.

[4] Michimasa Fujino. Design and development of the HondaJet. *Journal of aircraft*, 42(3):755–764, 2005.

[5] M. Kruse, T. Wunderlich, and Heinrich L. A conceptual study of a transonic NLF transport aircraft with forward swept wings. In *30th AAIA Applied Aerodynamics Conference, New Orleans, USA*, 2012.

[6] M Leatham, S Stokes, J Shaw, J Cooper, J Appa, and T Blaylock. Automatic mesh generation for rapid-response navier-stokes calculations. In *FLUIDS 2000 Conference and Exhibit*, page 2247, 2000.

[7] W. Pfenninger. Some results from the X-21 program. part 1- flow phenomena at the leading edge of swept wings(X-21 aircraft program results- laminar and turbulent boundary layer flow phenomena at leading edge of swept wings). *1965. 47 P*, 1965.

[8] G. Redeker and G. Wichmann. Forward sweep-a favorable concept for a laminar flow wing. *Journal of aircraft*, 28(2):97–103, 1991.

[9] A. Ronzheimer. Internal report. 2017.

[10] Geza Schrauf. Lilo 2.1 user's guide and tutorial. *Bremen, Germany, GSSC Technical Report*, 6, 2006.

[11] Dieter Schwamborn, Thomas Gerhold, and Ralf Heinrich. The DLR TAU-code: recent applications in research and industry. 2006.

[12] Arne Seitz, A Hübner, and Kristof Risse. The DLR tulam project: design of a short and medium range transport aircraft with forward swept NLF wing. *CEAS Aeronautical Journal*, 11(2):449–459, 2020.

[13] Antonio Sollo. P. 180 avanti: An iconic airplane and the achievement of an historical milestone. *Aerotecnica Missili & Spazio*, 100(1):69–78, 2021.

[14] Th. Streit, W. Bartelheimer, H. Bleecke, C-H. Rohardt, and W. Wohlrath. Design of a laminar wing for a commuter airplane using a 3D-design method. In *New Results in Numerical and Experimental Fluid Mechanics: Contributions to the 10 th AG STAB/DGLR Symposium Braunschweig, Germany 1996*, pages 319–326. Springer, 1997.

[15] Thomas Streit and Cornelius Hoffrogge. DLR transonic inverse design code, extensions and modifications to increase versatility and robustness. *The Aeronautical Journal*, 121(1245):1733–1757, 2017.

[16] Thomas Streit, Martin Kruse, Thomas Kilian, Judith V Geyr, and Ilias Petropoulos. Aerodynamic design and analysis of HLFC wings within the European project HLFC-WIN. In *ICAS 2022: 33rd Congress of the International Council of the Aeronautical Sciences*, 2022.

[17] Thomas Streit, Sven Wedler, and Martin Kruse. DLR natural and hybrid transonic laminar wing design incorporating new methodologies. *The Aeronautical Journal*, 119(1221):1303–1326, 2015.